The Thesis Committee for Isaac Michael Bodemann

Certifies that this is the approved version of the following Thesis:

Chemical Vapor Deposition of MoS_2 on Distributed Bragg Reflector for Room Temperature Polariton Condensation

APPROVED BY

SUPERVISING COMMITTEE:

Sanjay K. Banerjee, Supervisor

Deji Akinwande

Chemical Vapor Deposition of MoS_2 on Distributed Bragg Reflector for Room Temperature Polariton Condensation

by

Isaac Michael Bodemann

Thesis

Presented to the Faculty of the Graduate School of

The University of Texas at Austin

in Partial Fulfillment

of the Requirements

for the Degree of

Master of Science in Engineering

The University of Texas at Austin

December 2022

Acknowledgements

The past two years at The University of Texas at Austin has given me access to countless opportunities to grow and further my education. None of this would have been possible without the help of my dedicated professors, peers, research staff, and family. First, I would like to shine a light on my advisor, Professor Sanjay K. Banerjee, who assisted me over many hurdles and always provided with me the resources necessary to succeed. None of this research would have been possible without Professor Banerjee's leadership, and I am extremely grateful he accepted me with open arms as a member of his research group. Also, I would like to thank Professor Deji Akinwande. First, for agreeing to join my thesis committee. Second, for his 'Carbon and 2D Materials' course that shaped much of my understanding of 2D materials.

Next, I would like to thank my peers for helping me with the day-to-day struggles regarding research and academics. The members of Dr. Banerjee's lab group are all inspiring individuals. Each of them knows what it means to work tirelessly to achieve your goals. A special thank you to Matthew Disiena for going out of his way to assist me with roadblocks in my research and helping me with topics outside of my area of understanding. Without Matt's help I would not be where I am today. I would like to thank Jatin Singh and Dr. Ansh Ansh for lending me priceless advice and innovative ideas and techniques regarding CVD growth. Thank you, Chris Luth and Ryan Schalip, for being the first to make me feel welcome in Dr. Banerjee's group and showing me the ropes. Thank you, Dr. Sayema Chowdhury, for being a great mentor during my research experience for undergraduates in 2019. Sayema played perhaps the greatest role in shaping my understanding of the CVD growth of TMDs. Thank you, Dr. Anupam Roy, for welcoming my questions graciously and always being a reliable resource of expertise.

Of course, I would like to thank the lab staff at the Microelectronics Research Center for providing me with the necessary training to utilize the advanced tools available.

Thank you all for being accessible sources of information in times when I felt stuck using a tool. Thank you, Christine Wood and Melanie Gulick, for providing me the administrative assistance necessary to stay on track. Thank you, Professor David Snoke and Jonathan Beaumariage, from The University of Pittsburgh, for providing me with the concepts necessary to make this project possible. Their collaboration has been pivotal in the scope of this project.

Lastly, I would like to thank my family. Thank you, Mom and Dad, for providing the love, support, and invaluable lessons I needed to succeed. Thank you, Claire and Marcus, for being inspiring siblings. Thank you, Summer Coker, for being by my side for the past nine years. I am so grateful for your love, commitment, and for always lifting me up when I am at my lowest.

Thank you all for shaping me into the person I am today and for providing me with the tools, skills, and values to leave my mark on the world. I will be forever grateful for each moment spent at The University of Texas at Austin.

Abstract

Chemical Vapor Deposition of MoS_2 on Distributed Bragg Reflector for Room Temperature Polariton Condensation

Isaac Michael Bodemann, M.S.E.

The University of Texas at Austin, 2022

Supervisor: Sanjay K. Banerjee

The creation of a room temperature Bose Einstein Condensate has been the goal of much research since the phenomenon was first experimentally realized in 1995. Currently, polaritons stand out as a particularly viable option to achieve this goal as their low effective mass should in theory allow for a high condensation temperature. One proposed system to realize such a condensate is a semiconductor optical microcavity. In a semiconductor microcavity, distributed Bragg reflectors (DBR) are used to trap photons in the cavity, while a direct band gap semiconductor placed in the cavity would allow for the creation of excitons for those photons to couple with. In this work we explore the growth of crystalline monolayer Molybdenum Disulfide (MoS_2) directly onto the DBR to create such a microcavity. Growth of MoS_2 is well studied, however the DBR substrate presents unique challenges as the surface is inconducive for crystalline growth and the substrate itself warps and deteriorates at high temperatures. We then present techniques to overcome these challenges and recipes by which large area growth of monolayer MoS_2 growth on DBR can be attained.

Table of Contents

List of Figures

Chapter 1: Introduction

1.1 Bose-Einstein Condensation

Many areas of research, such as solid-state physics and materials science depend strongly on quantum mechanics, particularly with respect to cutting edge advancements in the electronics industry (Cohen). Understanding quantum mechanics plays a pivotal role in describing the behavior of subatomic particles and ultimately gave birth to the field of condensed matter physics (Cohen, find page #). Subatomic particles can be classified as either bosons or fermions depending on their spin. Bosons have integer spin (i.e. -1, 0, 1, …) while fermions have odd half-integer spin (i.e. –½, ½, …). Bose-Einstein statistics is used to describe particle systems consisting of bosons. The probability that a boson will occupy energy state ε_k is given by

$$f_{BE}(\varepsilon_k) = \frac{1}{e^{(\varepsilon_k - \mu)/k_B T} - 1}$$

where μ is the chemical potential and $k_B T$ is the thermal energy. It can then be shown that the fraction of particles in energy state ε_0, the ground state, is given by

$$\frac{n_0}{n} = 1 - \left(\frac{T}{T_c}\right)^{\frac{3}{2}} \; where \; T_c = \frac{2\pi\hbar^2}{k_B m}\left(\frac{n}{2.612}\right)^{\frac{2}{3}}$$

Therefore, if the temperature of a system of bosons is below the critical temperature (T_c) then a macroscopically significant number of bosons will occupy the ground state and will exhibit identical behavior; this is known as Bose-Einstein Condensation (BEC) [1].

This phenomenon provides a very interesting field of study, as Bose-Einstein condensates allow for microscopic quantum mechanics to be observed on a macroscopic scale. Typically, BEC only occurs in systems with very high densities or very low temperatures (nearing 0 Kelvin). Resultingly, the search for a near-room temperature BEC

system is of great interest within the field of condensed matter physics [2]. Most early cases of BEC were achieved using dilute atomic vapors; however, BECs have been created using molecules or quasi-particles. Quasi-particles are particularly promising regarding room temperature BEC thanks to hybrid particles of light and matter called polaritons. Polaritons grant controllable mass, repulsive interactions, and number conservation as opposed to a traditional photon, thus allowing a subatomic particle with no mass in free space to form a "superfluid of light"[3].

1.2 POLARITON CONDENSATION

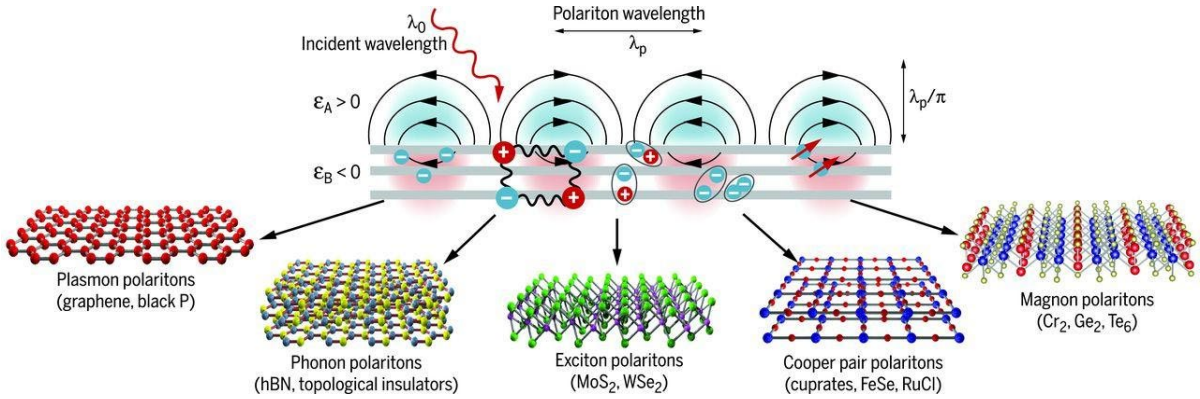

Figure 1: Types of Polaritons [4].

Polaritons are quasiparticles that form when light couples with an electric dipole, such as an exciton, phonon, or plasmon; examples of different polaritons formed from different types of electric dipoles are provided in figure 1 [4]. These polaritons may have different physical properties than their component particles. For instance, exciton polaritons exhibit an effective mass four orders of magnitude lower than a standalone exciton [1]. This reduction in mass provides a commensurate increase in the critical temperature, exemplifying the advantage of an exciton polariton condensate compared to

an exciton condensate. The challenge is thus to maintain a stable enough system of polaritons so that condensation may occur.

To generate a BEC of exciton polaritons, there must be a significant population of both photons and excitons. The photon population can be maintained using an optical cavity made from distributed Bragg reflectors (DBR). A distributed Bragg reflector is made of multiple layers of dielectric material with alternating high and low refractive indices. Reflected photons interfere with transmitted photons at each layer interface of the DBR material, generating transmission stop band. Therefore, when the wavelength of the incident light is within the stopband, the DBR acts as a highly reflective mirror [1]. When two DBRs are placed in parallel, they can create a cavity that traps photons at a certain wavelength. From the reflectance of the two DBR materials we can then estimate the cavity quality, Q as

$$Q \cong \frac{\pi (R_1 R_2)^{\frac{1}{4}}}{1 - (R_1 R_2)^{\frac{1}{2}}}$$

Physically, the cavity quality factor estimates the average number of round trips a photon will make in the cavity before escaping. For an ideal cavity, we would have $Q = \infty$, for practical purposes we simply need Q to be high enough for the photons to remain in the cavity long enough for polaritons to form [1].

If photons can equilibrate once trapped within this optical cavity, they acquire an effective mass and number conservation at a well-defined equilibrium temperature. However, even the highest quality cavities leak out photons so the supply must be continually replenished to maintain a constant population. While some DBRs can extend photon lifetimes to achieve equilibrium, full conservation of photons is not a requisite for BEC, and many quantum mechanical phenomena can be observed within partially equilibrated systems [2].

Direct bandgap materials can then be placed within the optical cavity to generate excitons, provided the bandgap energy can be overcome by the trapped photons. Since exciton lifetimes are typically very short (1-10 ps), a material that can generate multiple excitons within a small window of wavelengths would be ideal [5]. We chose Molybdenum Disulfide (MoS_2) as it is known for its strong exciton binding energy, large optical absorption in the visible range, and intense photoluminescence (PL) from its 677 nm direct bandgap peak [6]. Furthermore, the growth mechanisms of MoS_2 have also been well established to achieve large area, monolayer growth with chemical vapor deposition (CVD), a relatively accessible technique that is commonly used in materials research.

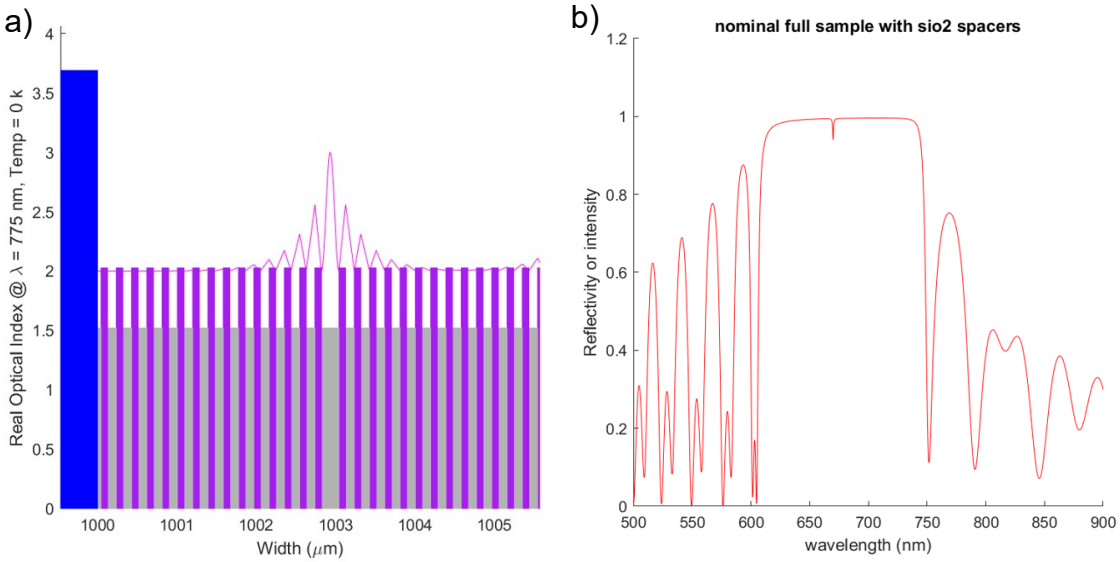

Figure 2: a) Reflection of photons as function of distance through the DBRs. Purple layers are Si_3N_4 and grey layers are SiO_2. b) Reflectivity at the center of the optical microcavity as a function of wavelength.

Our proposed system is designed to generate strong electric field confinement within the cavity and high reflectance in the exciton peak range of MoS_2. It consists of two 15-layer DBRs where each layer consists of 82.3 nm of Si_3N_4 on 110.1 nm of SiO_2 grown using CVD. Figure 2 provides simulations of the optical properties of the microcavity. The large node at the center of the microcavity in figure 2a is the electric field confinement which induces photon and exciton coupling. Figure 2b shows the high reflectance of photons with a wavelength between 600 and 750 nm, which is necessary to excite the 627 nm and 677 nm exciton peaks of MoS_2 monolayers [7]. The thickness of monolayer MoS_2 is around 0.7 nm, so it is considered negligible regarding the cavity length even when considering multiple layers separated by Al_2O_3 [8]. Fully realized, this system should allow for a polariton BEC to form at near room temperatures. The scope of this work is thus to optimize the growth of MoS_2 monolayers on the SiO_2/Si_3N_4 DBR.

Chapter 2: CVD Growth of MoS_2

2.1 Properties and Reaction Mechanisms

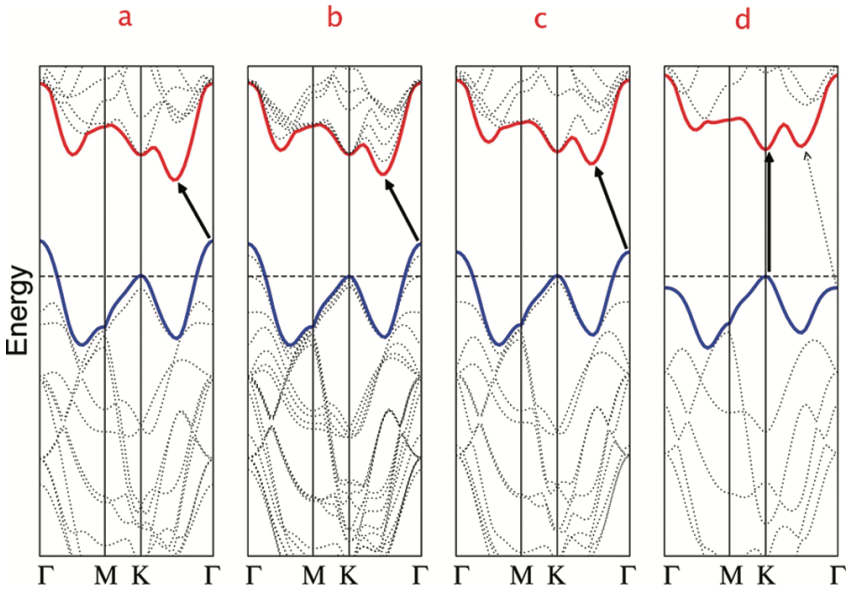

Figure 3: Band diagram of bulk, 4-layer, 2-layer, and 1-layer MoS_2 [7].

MoS_2 belongs to a class of 2D materials called transition metal dichalcogenides (TMDs). One interesting feature of many TMDs is their band alignment can shift from an indirect bandgap in few-layer/bulk to a direct bandgap in the monolayer [7]. Figure 3 illustrates this bandgap shift for MoS_2 as the number of layers are reduced. TMDs are composed of a transition metal atom (Mo, W, Nb, etc.) paired with two chalcogen atoms (S, Se, Te). Due to superior intralayer bonding relative to interlayer bonding, TMD monolayers can be obtained with relative ease. Exfoliation has been a popular technique to obtain monolayers of 2D materials, but it is inconsistent and lacks scalability. As mentioned earlier, CVD is another technique used to obtain monolayers of MoS_2 and can produce larger areas and higher quality films than other techniques. CVD growth of MoS_2

directly onto the DBR is ideal, as greater MoS_2 monolayer coverage will result in more excitons being generated by photons incident on the cavity. Additionally, multiple layers of monolayer MoS_2 can be grown to further increase exciton generation, provided the material used to separate the monolayers does not affect the optical gap of the cavity.

There are three known reaction pathways for the formation of MoS_2 with MoO_3 and S as precursors. The first reaction occurs when sublimated MoO_3 in the vapor phase reacts with sulfur vapor to form MoS_2.

$$4MoO_{3(v)} + 7S_{2(v)} \rightarrow 4MoS_{2(s)} + 6SO_{2(v)}$$

The next two reactions occur when MoO_3 is reduced to MoO_2. The second reaction occurs when MoO_2 vapor reacts with S vapor to form MoS_2 and the third occurs when crystallized MoO_2 on the substrate reacts with S vapor to form MoS_2 crystals [9].

$$4MoO_{2(v)} + 6S_{2(v)} \rightarrow 4MoS_{2(s)} + 4SO_{2(v)}$$

$$4MoO_{2(s)} + 6S_{2(v)} \rightarrow 4MoS_{2(s)} + 4SO_{2(v)}$$

H_2 gas can also be introduced to increase MoO_3 reduction and inhibit the thermal etching effect to promote the growth of polycrystalline monolayer MoS_2 films [10], [11].

There are three crystal configurations of MoS_2: 1T, 2H, and 3R. Figure 4 shows the difference between these configurations. The crystal alignment can affect the electrical properties, as 1T-MoS_2 is metallic while 2H/3R-MoS_2 are semiconducting. CVD grown, crystalline MoS_2 is composed of the 2H phase. The 1T configuration is usually only stable at low energies but becomes relevant in amorphous MoS_2 [12], [13]. The 3R configuration is only present in specific, unrelated growth environments [14], [15].

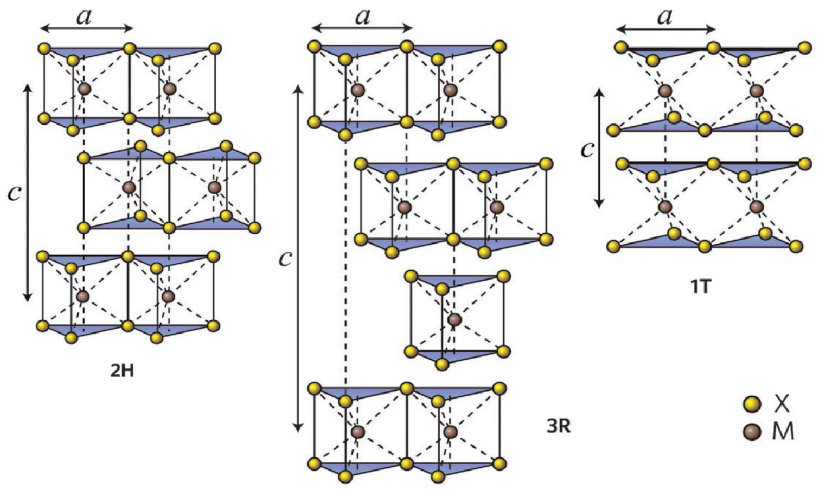

Figure 4: Interlayer crystal alignment of different MoS_2 configurations. Atom M represents Mo and atom X represents sulfur [12].

2.2 MoS_2 Grown on Si/SiO_2 Substrates

The growth of MoS_2 on polished Si/SiO_2 substrates has been well studied, providing a useful reference for calibrating growth parameters in our system. A schematic of our CVD reactor is shown in figure 5 and photos of the system are included in the appendix as figures A.2.1 - A.2.3.

A two-zone furnace system was used. The molybdenum oxide (MoO_3) precursor is loaded in the primary zone of the furnace, while the sulfur (S) precursor is loaded in another zone upstream wrapped with a separate heater. The furnace is attached to argon (Ar), nitrogen (N_2), and hydrogen (H_2) gas lines, as well as a low vacuum pump and atmospheric pressure valve. The process chamber is kept under vacuum while in an idle state to prevent moisture from accumulating but is operated under atmospheric pressure. For this project, atmospheric pressure chemical vapor deposition (APCVD) is used.

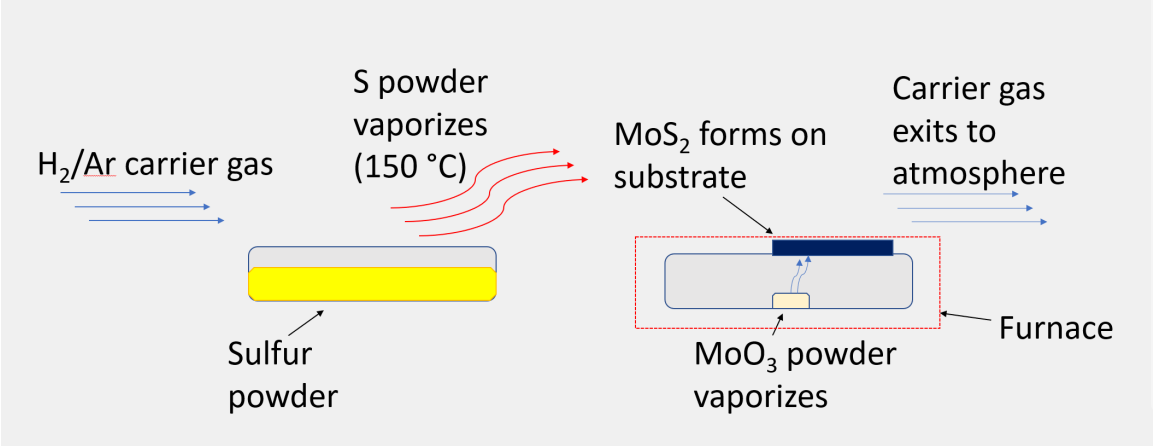

Figure 5: Diagram of CVD reactor.

The growth process is performed as follows. First, approximately 8 – 12 mg MoO_3 (Millipore Sigma, >99.5%) weighed and added to an alumina crucible in a single, compact area towards the center of the boat. Next, the growth substrate is placed directly onto this boat, lying directly above the MoO_3, with the sample oriented slightly downstream of the MoO_3. A second boat is then filled with >100 mg sulfur (Acros Organics, 99.999%). The process chamber is opened to atmosphere and the sample/MoO_3 boat is loaded, followed by the sulfur boat. Next, the process chamber is thoroughly purged to remove any moisture that might have been introduced when the samples were loaded. This is done by flowing 200 sccm of N_2 and 100 sccm of Ar through the tube while the vacuum valve is opened. After ~10 minutes of purging, the gas flow valves are closed, and the pressure is recorded. This value can be compared to the system's base pressure to estimate the quantity of residuals remaining in the system; a difference of 1 mTorr or less is preferable. Once the system is purged, the chamber is backfilled with N_2 and Ar until it reaches atmospheric pressure, then the atmosphere valve is opened. This is done to ensure no moisture is introduced into the system when the atmosphere valve is opened. The reaction and carrier gasses are then introduced (in this case H_2 and Ar) and the furnace is heated to the specified growth temperature. The sulfur heater is turned on while the furnace is heating; when the

heater is turned on determines if the reaction environment is S-rich/S-deficient once the growth temperature is reached. Once the furnace has reached the growth temperature, it is held there for the duration of the growth. After the growth has completed, the furnace chamber is opened and cooled naturally. Once the furnace has cooled below the reaction temperature, the sulfur heater and H_2 gas flow are turned off. The sample is removed from the chamber once it has thoroughly cooled.

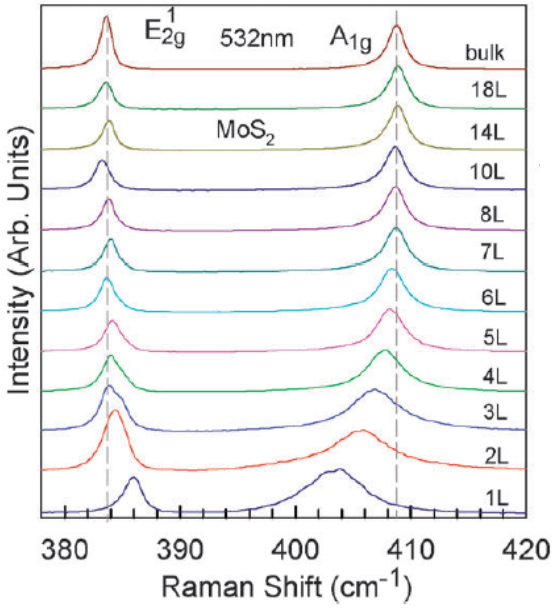

Figure 6: Raman spectra of exfoliated MoS_2 with varying thicknesses [12].

The sample is first characterized using optical microscopy to examine if any notable MoS_2 growth can be seen. Then, Raman spectroscopy (Raman) and photoluminescence spectroscopy are conducted to determine the crystal and optical quality of the grown material. Raman and PL can also both be useful in determining the layer thickness of MoS_2. Monolayer MoS_2 has an in-plane vibration (E^1_{2g}) peak at ~385 cm^{-1} and out-of-plane vibration peak (A_{1g}) at ~404.5 cm^{-1} [16],[17]. The E^1_{2g} peak experiences a red shift as the number of layers increase, while the A_{1g} peak experiences a blue shift. The distance

between the two peaks can thus be used to determine the thickness of MoS_2. CVD grown monolayer MoS_2 usually has a Raman peak difference ~19.5 cm^{-1} [12]. Figure 6 shows the Raman peak difference reducing with number of layers for MoS_2. It should be noted that exfoliated and CVD grown MoS_2 monolayers show slightly different Raman peak differences (~19.4 cm^{-1} to ~20.4 cm^{-1}). This is likely due discrete grain boundaries being more prominent in CVD grown MoS_2 [18].

PL can then be used to determine the optical absorption of the MoS_2 and further confirm the crystal quality. Monolayer MoS_2 is known for showing A1 and B1 exciton peaks as it transitions from an indirect to direct bandgap material with reducing layers. The A1 peak is usually located at ~1.83 eV (677 nm) and the B1 peak at ~1.97 eV (627 nm) [7],[19]. These peaks often shift slightly based on the preparation and quality of the samples. It should also be noted that the A1 peak is generally much sharper and more intense than the B1 peak. Figure 7a shows the PL peaks of exfoliated monolayer MoS_2 on a Si/SiO_2 substrate. Figure 7b gives the PL reading of our grown MoS_2 on a Si/SiO_2 substrate. The small peak difference can be attributed to a greater population of defects within CVD grown MoS_2 relative to exfoliated [20]. Our Raman data from our MoS_2 on Si/SiO_2 can be found in the appendix (A.2.4) with peaks at 382 and 400 cm^{-1} (peak difference of 18 cm^{-1}), which is consistent with reports for monolayer MoS_2 [12], [21].

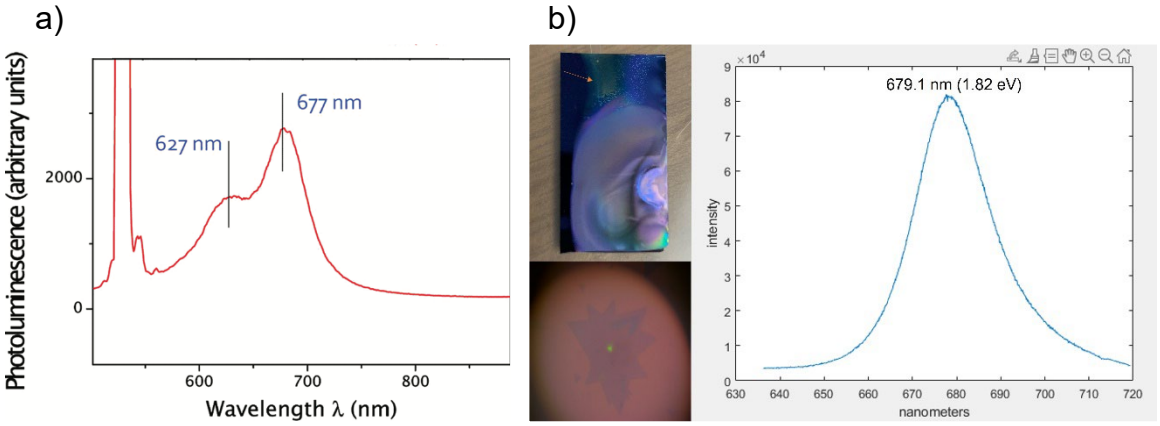

Figure 7: a) PL reading of exfoliated MoS_2 monolayer on Si/SiO_2 sample. Exciton peak A1 is shown at 677 nm (1.83 eV) and exciton peak B1 is shown at 627 nm (1.97 eV) [7]. b) PL reading of MoS_2 monolayer on Si/SiO_2 sample from our optimized growth recipe with exciton A1 peak at 679.1 nm (1.82 eV).

The optimal growth parameters for our system on polished SiO_2 substrates are as follows. Growth temperature of 750 ºC for 10 minutes, H_2 flow rate of 3 sccm and Ar flow rate of 6 sccm. The sulfur heater is set to 150 ºC and is turned on when the furnace reaches 400 ºC. The back of the sample is placed approximately 20 cm downstream the sulfur source, near the center of the furnace. Approximately 8 – 12 mg of MoO_3 is loaded into the boat holding the sample. Other growth recipes were attempted in prior work by varying the temperature, growth time, MoO_3 mass and gas flow rates to optimize large area MoS_2 monolayer coverage.

Chapter 3: MoS_2 Growth on DBR

3.1 Initial Challenges

MoS_2 growth on the DBR substrate was first attempted using the recipe optimized for growth on the Si/SiO_2 substrate; however, the DBR substrate began to warp dramatically when held at high temperatures. This leads to serious problems, such as surface fracturing and expulsion of DBR layers. Figure 8 illustrates the deterioration of the DBR material under the conditions of the recipe optimized for growth on Si/SiO_2 substrates. As mentioned earlier, our DBR material is composed of alternating layers of CVD grown SiO_2 and Si_3N_4. These materials have different coefficients of thermal expansion so as they reach high temperatures the layers will shift unevenly, causing the substrate to fracture and warp [22]. This issue is unavoidable as with all large-area growth techniques known for MoS_2, temperature and coverage/crystallinity are a common tradeoff. Therefore, our focus was to optimize the growth of MoS_2 on the DBR substrate without allowing the substrate to significantly warp or fracture.

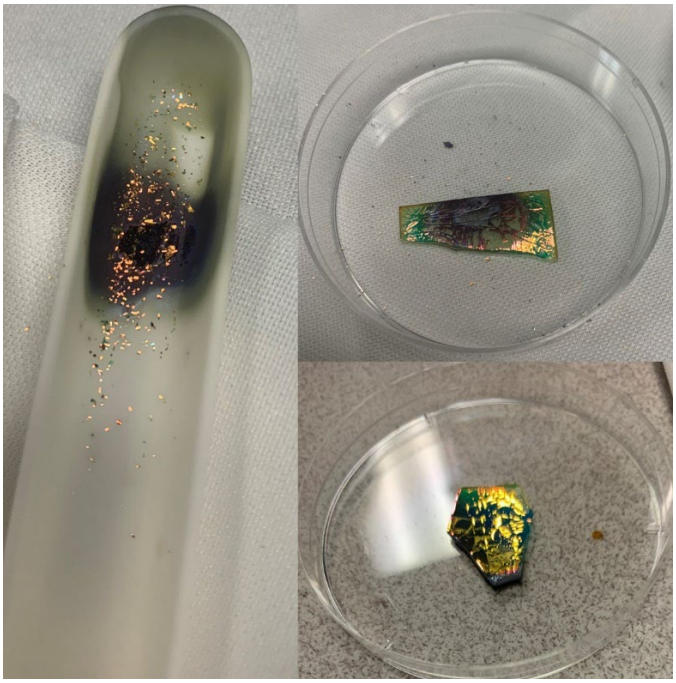

Figure 8: Breakdown of DBR substrates. Left: DBR materials emitted from the substrate into the growth boat. Top right: Warped DBR substrate with missing DBR materials and fracturing. Bottom right: Fracturing seen by varying light refraction across DBR surface.

First, we tried lowering the ramp rate of the temperature of the system to alleviate thermal shock, however this did little to preserve the integrity of the DBR substrate. We determined that the substrate begins significantly warping while it is held at the growth temperature, not while ramping up. The obvious next step was to decrease the growth temperature. At this point we began to add SiO_2 samples to the growth chamber in a separate boat downstream of the DBR boat to track the growth of MoS_2 on a familiar substrate. However, we were unable to find a growth temperature that allowed for the nucleation and crystallization of MoS_2 without heavily damaging the DBR.

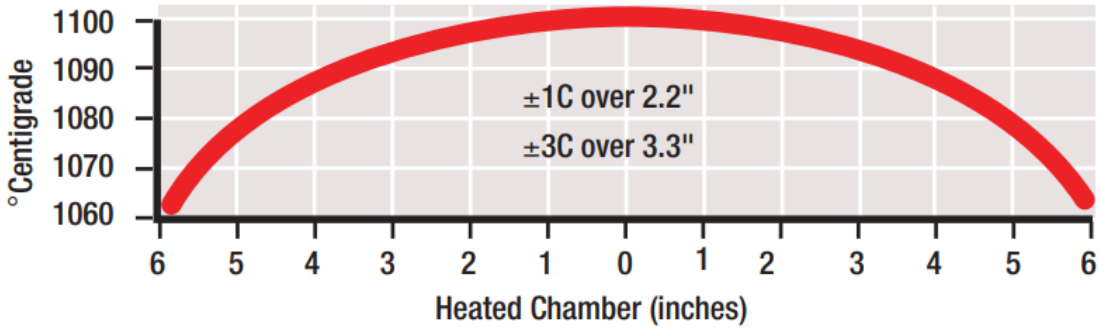

Figure 9: Temperature variation across length of tube furnace [23].

Next, different spots in the furnace were tested. It was discovered that moving the DBR boat to a far edge of the furnace dramatically reduced the warping. A temperature distribution of the furnace was found and used to relate the position of the DBR to the temperature. The new boat location is approximately 5 inches to the left of center using figure 9 as reference. However, this decrease in temperature was not the reason for the preservation of the DBR, as we tested the DBR in the original furnace position at this lower temperature and it resulted in thorough deterioration. We speculate that as the center of the furnace overshoots the max temperature and drops, the rate of thermal expansion on the materials is intense enough to cause major fracturing. However, we believe the outside atmosphere may act as somewhat of a damping agent on the edge of the furnace. Thus, any heat fluctuations in the furnace would be less intense near the edge as they are mitigated by the outside atmosphere, leading to less fracturing of the substrate. Figure 11 shows the difference between the two positions within the furnace (namely 8 cm and 20 cm downstream of the sulfur supply). While the sample at the new furnace position of 8 cm still experiences cracking, it is significantly less destructive to the DBR and retains large, continuous areas of material.

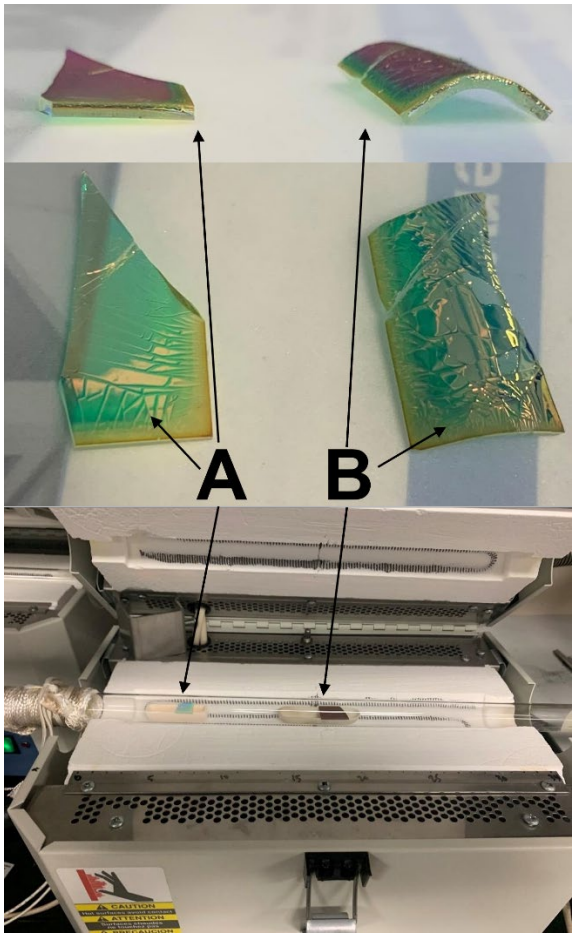

Figure 10: Effect of furnace position on the warping of DBR. Bottom: Furnace positions of each sample. Middle: Surfaces of both DBR substrates. Top: Horizontal view of DBR substrates to compare warping.

While this step improved the growth process with respect to the preservation of the DBR substrates, there were still significant issues regarding the quality of MoS_2 on the surface. The MoS_2 grown on the DBR was often amorphous instead of the usual crystalline domains seen on Si/SiO_2 substrates. This is an issue regarding exciton generation, as amorphous MoS_2 (a-MoS_2) does not generate excitons as reliably as crystalline MoS_2 (c-MoS_2); Figure 11a shows the weakened exciton peaks of the amorphous MoS_2. This is due

to the 1T' phase being prevalent in a-MoS_2 while c-MoS_2 is comprised entirely of the 2H phase [13]. Therefore, c-MoS_2 provides a more reliable supply of excitons. Crystalline MoS_2 did form on the DBRs, but only in bulk and therefore provided no significant PL peak. Figure 11b shows the bulk MoS_2 grown and the corresponding Raman data [24].

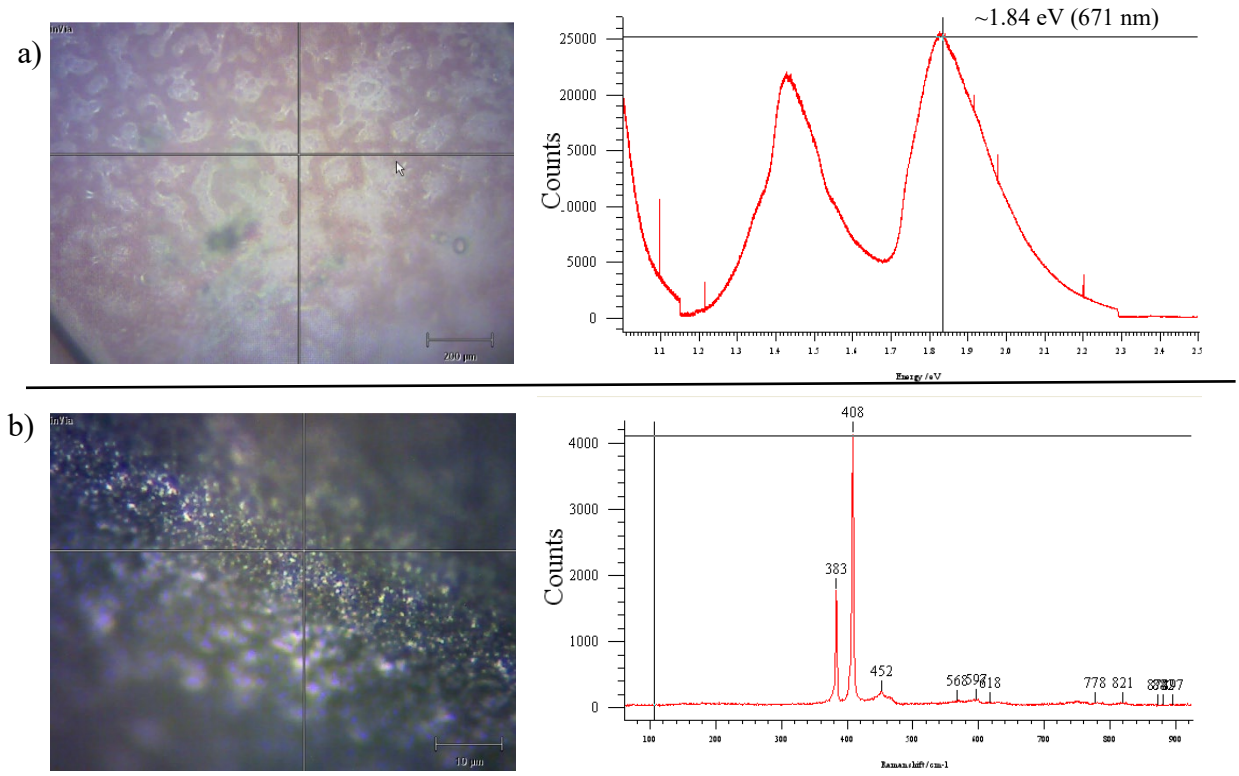

Figure 11: a) Optical microscope image of MoS_2 and PL data of corresponding region. MoS_2 amorphous areas (light blue/green) on DBR (darker purple). b) Optical microscope image of MoS_2 crystal with corresponding Raman data. Raman data of corresponding region showing bulk MoS_2 peaks. Other peaks are likely due to noise or impurities.

At this point we were able to preserve the DBR substrates while also attaining some form of MoS_2 growth. The next challenge was thus to acquire crystalline MoS_2 monolayers that could generate a satisfactory population of excitons.

3.2 Depositing Al_2O_3 onto the DBR Surface

Originally, the surface of the DBR, namely the "spacer layer," was comprised of CVD grown SiO_2. This is not the same as the polished SiO_2 that makes up the surface of the Si/SiO_2 substrates we normally use. Compared to the polished SiO_2 surface of our Si/SiO_2 substrates, the CVD grown SiO_2 of the DBR does not have a smooth surface for MoS_2 to align with during nucleation. This results in amorphous MoS_2 instead of crystalline. To alleviate this issue, we deposited Al_2O_3 on the surface of the DBR using atomic layer deposition (ALD), as we have experience growing MoS_2 on $Al_2O_3/Si/SiO_2$ substrates. The only constraint is that the Al_2O_3 must also be thin enough to avoid creating optical band misalignment in the microcavity. It was determined that up to 20 nm was allowable, so Al_2O_3 thicknesses of 1, 5, 10 and 20 nm were all examined.

The ALD growth of Al_2O_3 was done using alternating pulses of trimethylaluminum, $Al_2(CH_3)_6$, and water at 250 °C. $Al_2(CH_3)_6$ reacts with water to form Al_2O_3 and methane gas. The precise reaction is given below. Each cycle produces 1 angstrom of Al_2O_3 [25].

$$Al_2(CH_3)_6 + 3H_2O \rightarrow Al_2O_3 + 6CH_4$$

CVD growth on 1 nm of Al_2O_3 showed little difference compared to growth directly onto the DBR. CVD growth on 5 nm of Al_2O_3 was the first to show promising results. Crystalline MoS_2 domains, visually alike to those grown on Si/SiO_2 substrates, could be seen through the optical microscope. Figure 12 provides images of these domains. It is apparent that the MoS_2 achieved large area coverage in the photographed regions. Thicker areas of MoS_2 can be identified by the blue areas with brighter colors, while monolayer/few-layer areas show faint contrast to the surface. The MoS_2 domains don't

appear to have highly ordered crystallinity since most edges are not very sharp, but it is significant progress compared to the amorphous MoS_2 grown earlier on the DBR. This sample was shipped to a collaborative group, as our PL and Raman tool was under maintenance, where they performed PL and gathered reflectivity data. Both these measurements yielded promising enough results to move forward with growth of the top DBR layers for microcavity testing. The PL data for this sample can be found in the appendix (figure A.3.1).

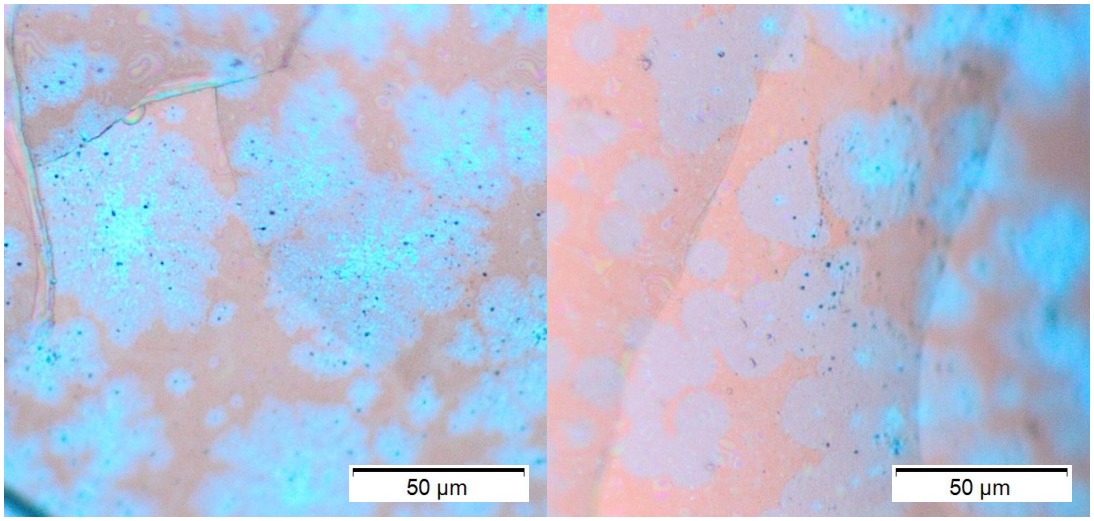

Figure 12: Optical microscope images of MoS_2 on DBR with 5 nm Al_2O_3. The MoS_2 domains are blue while the Al_2O_3/DBR is orange/pink.

Next, DBR samples with 10 nm of Al_2O_3 were tested, but they showed little difference compared to the 5 nm samples. MoS_2 growth was then done on DBR samples with 20 nm of Al_2O_3. Figure 13 provides optical images of the sample. The MoS_2 domains appeared relatively similar in shape but were slightly smaller. There was a clear shift in the abundance of islands, which can be seen as the dark grey dots on top of the white/light blue few-layer domains. The contrast of the domains becomes sharper/darker as the layer

thickness increases, often showing very dark MoO_x islands. We decided to proceed by depositing 5 nm of Al_2O_3 on top of the DBRs as no noticeable improvements in growth were obtained by increasing the thickness of the Al_2O_3 past 5 nm.

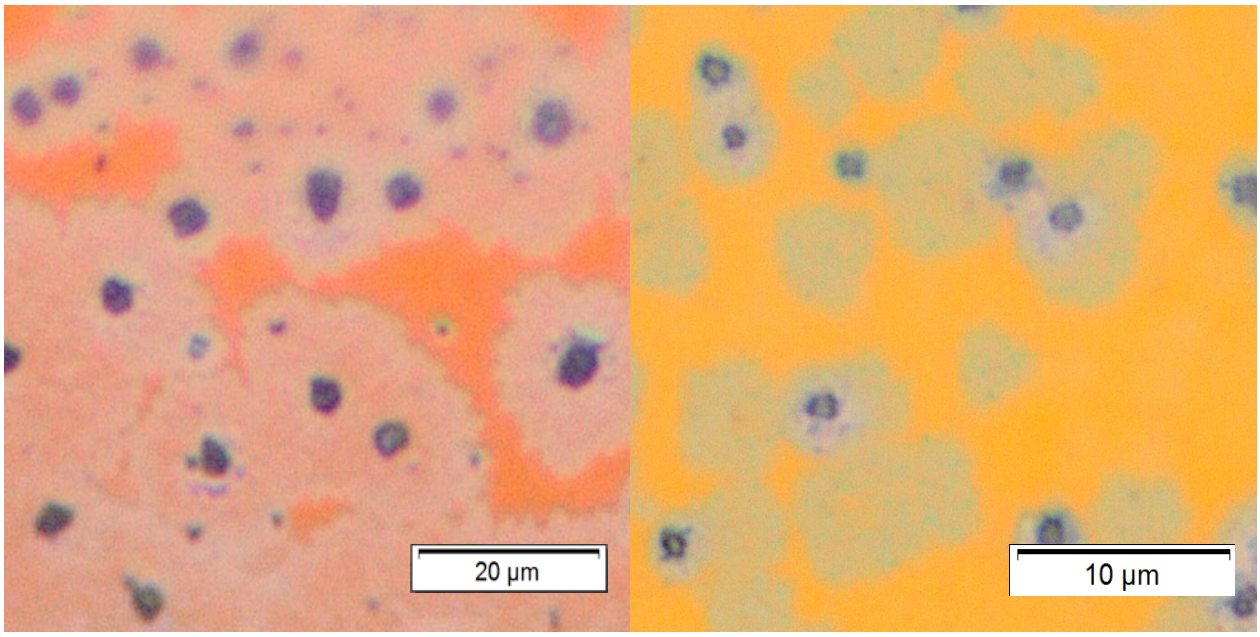

Figure 13: Optical microscope images of MoS_2 on DBR with 20 nm Al_2O_3. The MoS_2 domains are light blue and white while the DBR/Al_2O_3 has an orangish hue.

The substrates with MoS_2 grown on 20 nm of Al_2O_3 were then used as test samples for conducting layered growths of MoS_2. A 1 nm Al_2O_3 layer was deposited onto the MoS_2 layer followed by another MoS_2 growth. This process was then repeated for a 3rd MoS_2 layer. Images of the surface after each growth step are provided in figure 14. After the 2nd growth, the MoS_2 domains became much sharper, and coverage increased. The same phenomenon was observed to occur after the 3rd growth.

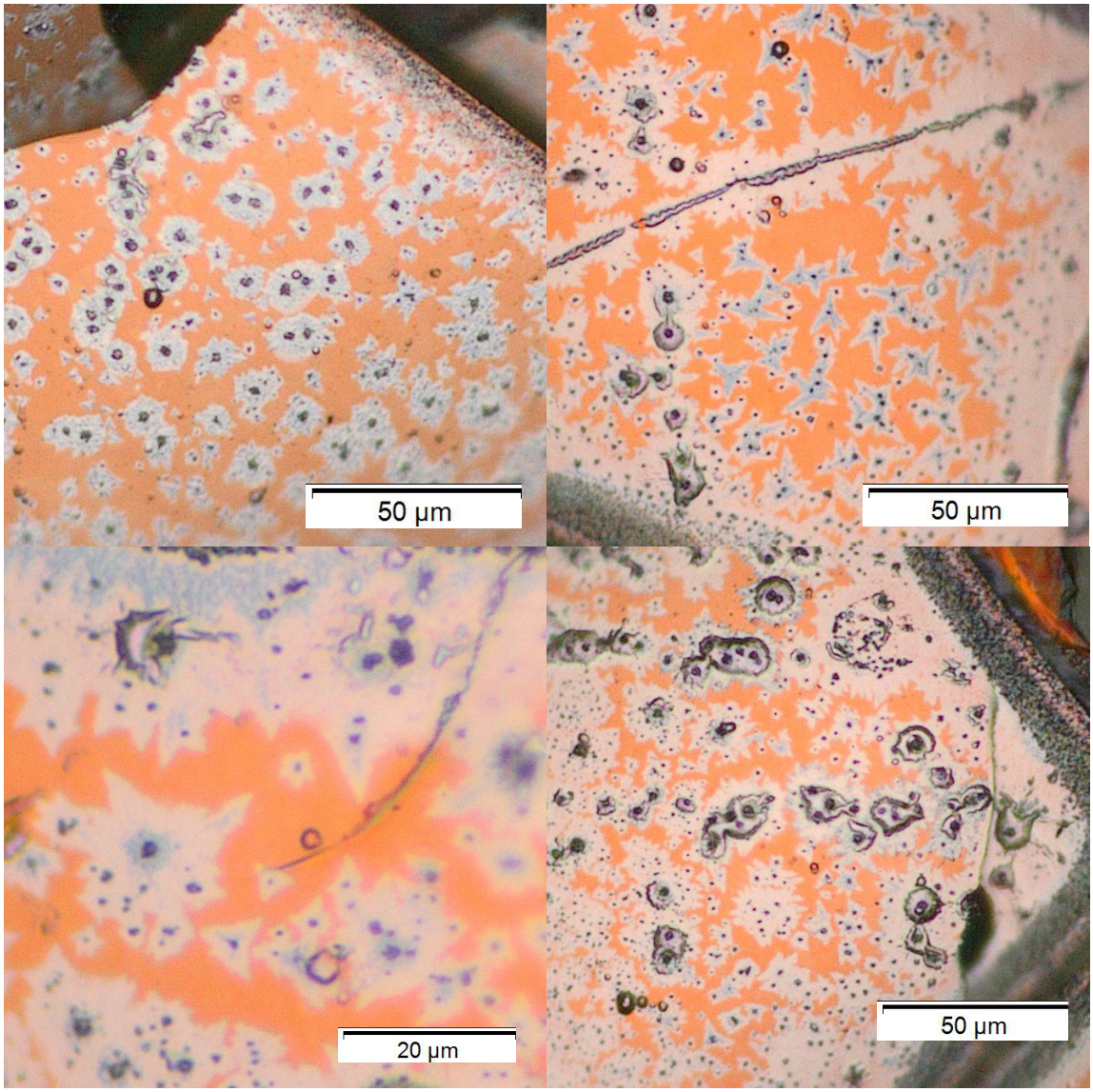

Figure 14: Optical microscope images of MoS_2 on DBR with consecutive Al_2O_3 and MoS_2 depositions. The MoS_2 domains are white/grey while the DBR/Al_2O_3 is an orangish hue. Top images are after 2nd consecutive MoS_2 growth. Bottom images are after 3rd consecutive MoS_2 growth. 1 nm Al_2O_3 was deposited after 1st and 2nd MoS_2 growths.

With each growth step the sample would deteriorate further and the domains became larger. More than 1 nm of Al_2O_3 will be necessary to create a continuous film over the deposited MoS_2. This is due to Al_2O_3 strongly preferring nucleation at the grain boundaries of monolayer MoS_2 films leading to incomplete Al_2O_3 coverage over the grown MoS_2. Figure 15 exemplifies this effect. Unfortunately it has been shown that at least 20 nm of Al_2O_3 must be deposited to isolate the MoS_2 layer [26].

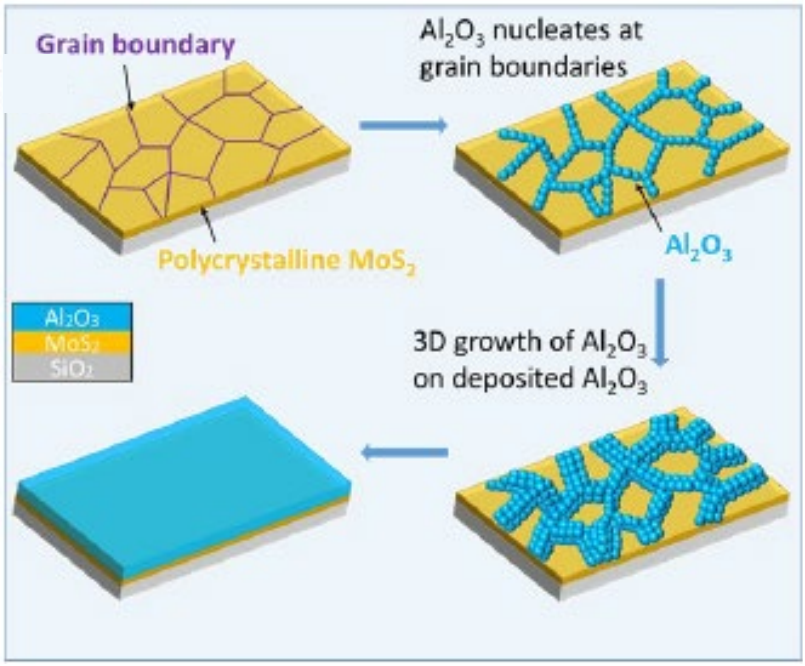

Figure 15: Diagram of ALD Al_2O_3 deposited onto polycrystalline MoS_2 [26].

3.3 Salt Assisted MoS_2 Growth

The final major technique introduced was salt assisted growth of MoS_2 as it has been found that MoO_3 reacts favorably with salts MX (M = Na, K; X = F, Cl, Br, I). The

cation M forms molten droplets of M-Mo-O with a low melting temperature of T_{melt} = 605 ºC corresponding to $Na_2Mo_2A_7$. The anion X forms metal oxyhalides with a low melting temperature of T_{melt} = 175 ºC corresponding to MoO_2Cl_2 [27]. The possible reaction that corresponds to the lowest melting point for salt assisted MoS_2 growth is as follows

$$3MoO_3(s) + 2NaCl(s) \rightarrow Na_2Mo_2O_7 + MoO_2Cl_2(g)$$

The full reaction table is provided in the appendix as figure A.3.2. NaCl (Sigma Aldrich, 99.999%) was added to the MoO_3 powder loaded underneath the DBR or Si/SiO_2 samples. It is crucial to thoroughly integrate the salt with the MoO_3 otherwise there will be unreacted MoO_3 left over in the boat. The salt to MoO_3 ratio gives the lowest reaction point at ~59% MoO_3 by mass, as seen by figure A.3.3 in the appendix [27]. However, in practice this ratio was found to oversaturate the system with Mo, causing large crystals of Mo to form even below the eutectic point (~655 ºC). Different ratios were tested but a ratio of ~70% MoO_3 by mass was found to give the best results for our system.

To optimize the salt assisted growth, we tested growths at various temperatures between 600 and 700 ºC. Additionally, the growth time was increased from the original recipe's 10 minutes to 20 minutes to accommodate lateral expansion and large area coverage of MoS_2 domains at the lower growth temperature. Higher temperatures led to increased warping of the DBR, but the increased time at the maximum temperature had no adverse effect on the DBR substrates.

Interestingly, the MoS_2 seemed to prefer lateral growth and many domains formed off bulk MoO_x crystals bonded to the Al_2O_3 layer. MoS_2 also seemed to readily form a large crystalline film. Figure 16a shows domains at the outer region of the film. Ultimately

this is ideal, as crystalline monolayer films of MoS_2 are preferred for optimal exciton generation. Raman data confirmed that crystalline MoS_2 was present, but the MoS_2 was generally thicker in these films than preferred. The Raman data can be found in figure 16b. Note that the Raman spectrum for a blank DBR produces a linearly increasing Raman spectrum and can be found in the Appendix as figure A.3.4. From the peak difference (~24.5 cm^{-1}), it seems these domains were ~3 layers thick [12], [17]. This is likely due to an abundancy of Mo. We decided to increase the temperature of the S heater from 150 to 160 ºC to match this abundance of Mo and promote lateral growth. Also, with a new shipment of DBRs, we were requested to deposit the spacer layer ourselves. Originally it was ~110 nm SiO_2, but we deposited 102 nm Al_2O_3 and forewent the additional 5 nm Al_2O_3 we were adding prior. Figure 17a shows a thin film area with very little contrast to the surface but visible grain boundaries [28]. Raman data from figure 17b confirms that the layer thickness was reduced, as the peak difference is ~21 cm^{-1} [12], [16].

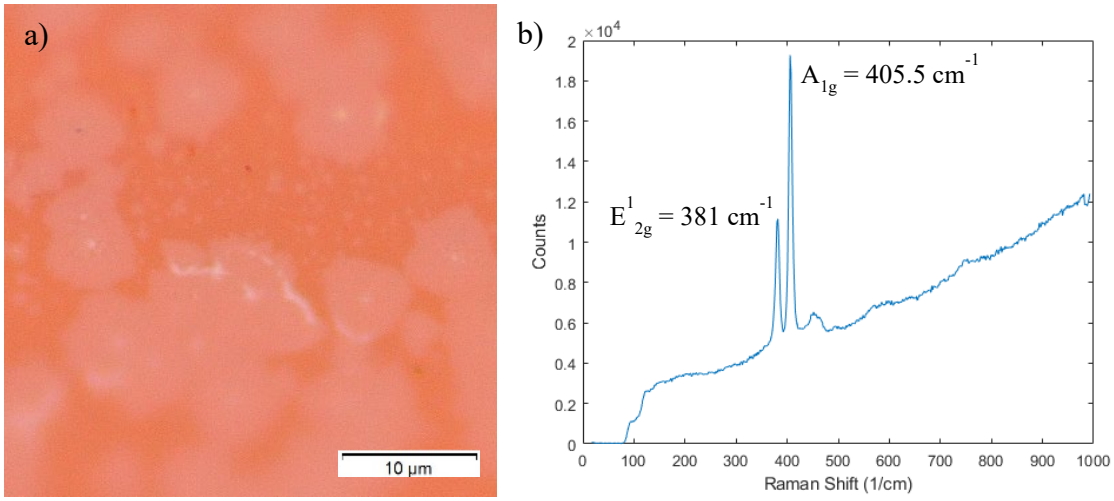

Figure 16: a) Optical microscope image of MoS_2 domains on DBR with 5 nm Al_2O_3 after salt assisted growth. Pale white areas are few layer MoS_2 domains, and the dark orange area is DBR/Al_2O_3. b) Raman data of corresponding region.

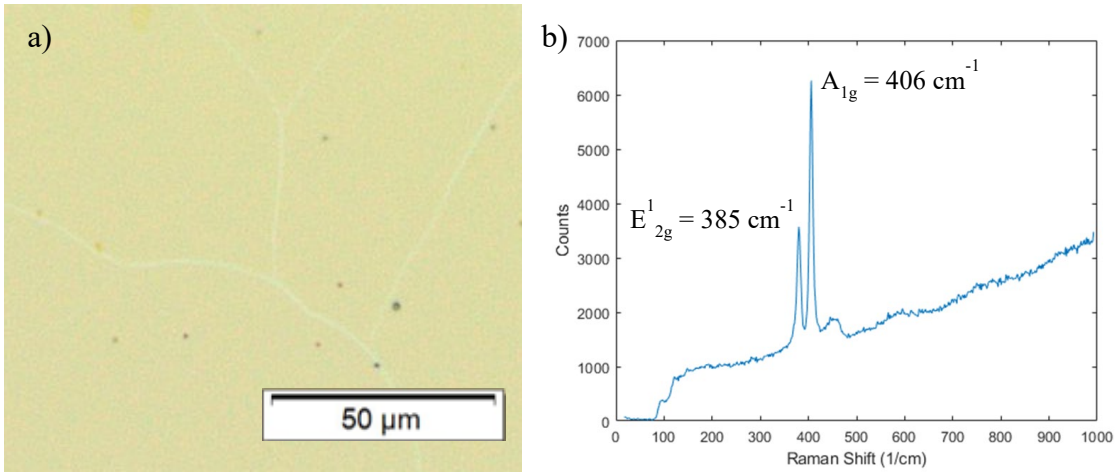

Figure 17: a) Optical microscope image of thin crystalline film MoS_2 on DBR with 102 nm Al_2O_3. Grain boundaries (white lines) of polycrystalline MoS_2 can be seen. b) Raman data of corresponding region.

Monolayer MoS_2 growth was found to be most prevalent when the temperature of the system was increased to 675 ºC, the carrier gas (Ar) flow rate was increased to 10 sccm, and the H_2 gas flow rate was increased to 4 sccm. These values seem to be the optimal spot for adatom mobility and crystalline film formation. Figure 18a gives an image of a domain populated region, while most areas were covered with a continuous film of expanded domains. Figure 18b gives the corresponding Raman spectrum, confirming the presence of MoS_2 monolayers with a peak difference of 19.5 cm^{-1} [12],[16].

Our optimized recipe is thus: 14.5 mg MoO_3; 4.5 mg NaCl. DBR boat 8 cm downstream of S boat. H_2 flow rate at 4 sccm; Ar flow rate at 10 sccm. Furnace temperature set to 675 ºC and left at max temperature for 20 minutes. S heater set to 160 ºF and turned on when the furnace temperature reaches 200 ºC. System at atmospheric pressure, but the chamber must be purged within 1 mTorr of the vacuum pressure.

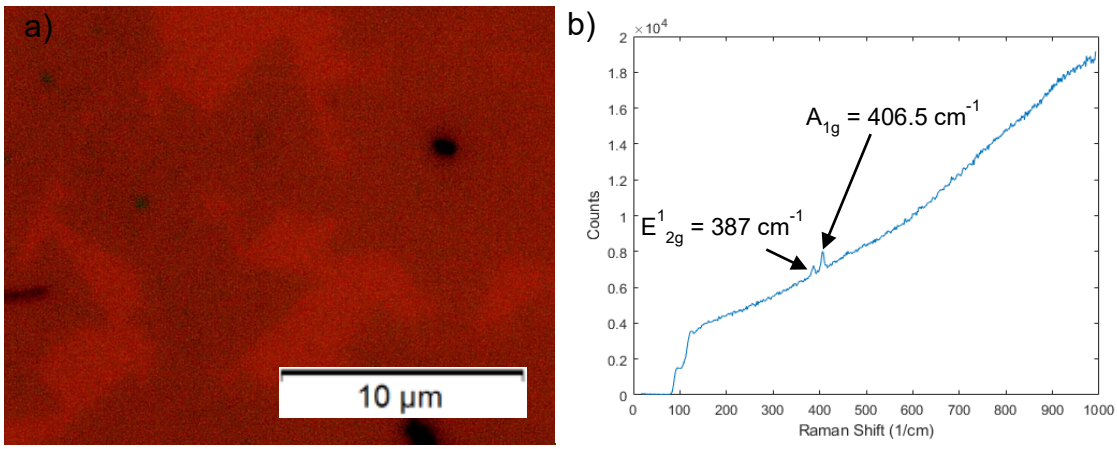

Figure 18: a) Optical microscope image of MoS_2 monolayer domains on DBR with 102 nm Al_2O_3. The monolayers are dark red with triangular edges, the DBR/Al_2O_3 surface is lighter red, and the black specs are bulk MoO_x crystals. b) Raman data of corresponding region.

Chapter 4: Conclusions and Future Work

Since the DBR materials are vulnerable to high temperatures, they have proven to be very challenging substrates for CVD growth. In this research, innovative techniques were utilized to alleviate stress to the material and generate large areas of few-layer, crystalline MoS_2 films. Thermal stress on the DBR samples was reduced by relocation of the boat within the furnace. ALD deposited Al_2O_3 was introduced to the surface to promote the growth of crystalline MoS_2 instead of amorphous MoS_2. Salt-assisted growth was utilized to further reduce the thermal stress on the substrate and promote the large area growth of crystalline MoS_2 films. Using these techniques, we were able to produce large area growth of monolayer MoS_2 on DBR substrates while preserving the integrity of the DBR.

We suggest that future research focus on growing consecutive layers of MoS_2 monolayers onto the same DBR substrate. Stacking monolayers of MoS_2 may prove a difficult task as it has been found that ALD Al_2O_3 tends to nucleate at grain boundaries of MoS_2 [26]. Therefore, depositing only 1 nm of ALD Al_2O_3 to separate MoS_2 monolayers may not be possible without some form of functionalization; approximately 20 nm of Al_2O_3 must be deposited to create a closed film over the MoS_2 film [26]. We propose that a new technique be implemented since we are growing the spacer layer within our lab. A large portion of the spacer layer (>= 20 nm) could be grown, followed by the first MoS_2 growth. Another large portion of the spacer layer could be grown followed by another MoS_2 growth. This process could be repeated to ensure that there is enough Al_2O_3 being deposited to negate issues arising from holes within the Al_2O_3 film. Approximately 5 layers would be possible based on this theory, which would hypothetically generate 5 times as many excitons as a single layer of MoS_2 monolayers.

To address the issue of bulk molybdenum on the DBR surface, we propose the implementation of a sacrificial Si/SiO_2 sample present on the same boat. This sample

would capture most of the excess MoO_x while the rest would flow downstream to bind to the DBR's surface. MoS_2 growth using the CVD setup proposed in this research typically leads to a coffee ring effect. The inner ring consists of bulk Mo and MoS_2 thicknesses will decrease as you move outwards from this ring. Appendix figure A.4.1 illustrates this effect for both a regular and salt assisted CVD growth of MoS_2. Salt assisted growth drastically increases the coffee ring effect. The DBR should be placed in the outer ring area to minimize the amount of deposited MoO_x and promote the growth of a large monolayer MoS_2 film.

In conclusion, the CVD growth of MoS_2 on DBRs is still in the early stages and can be improved to promote exciton generation and photon-exciton coupling; however, this work has made great strides in the early research and development of a near-room temperature BEC by utilizing novel growth approaches.

Appendix

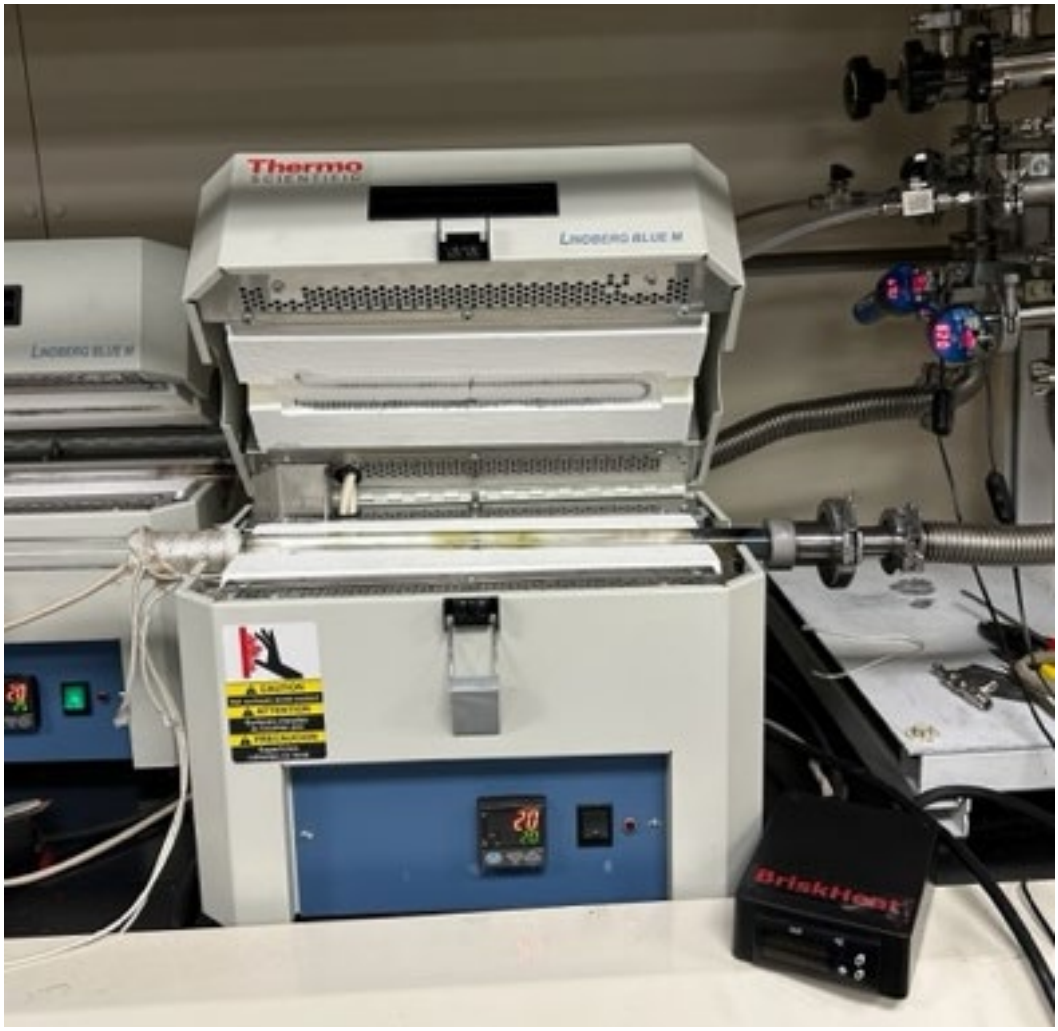

Figure A.2.1: Image of CVD growth furnace. Inlet gas line is to the left and atmosphere/vacuum valves are to the right. The sulfur heater is wrapped around the tube on the left. The furnace in the back is used for selenium-based TMDs.

Figure A.2.2: Gas flow controllers and corresponding valves.

Figure A.2.3: Vacuum and atmospheric valves with pressure gauge.

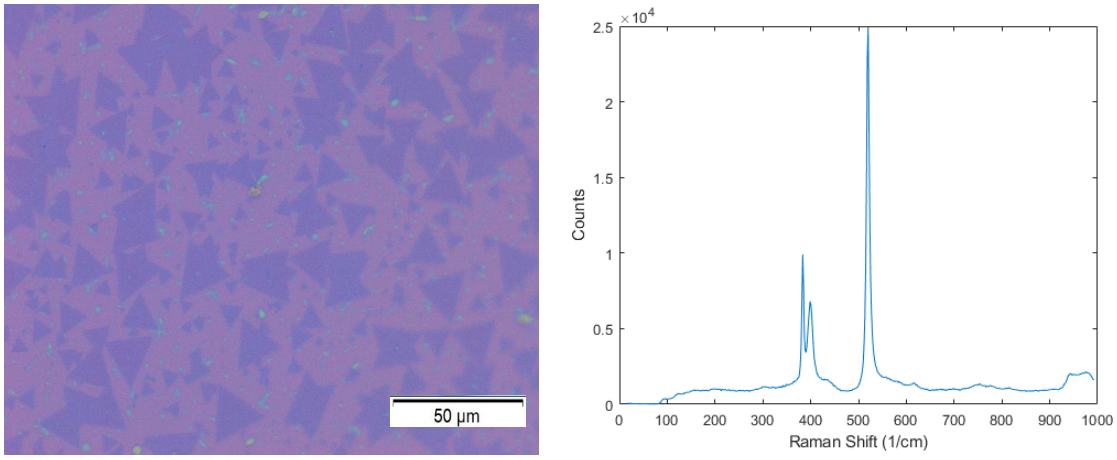

Figure A.2.4: MoS_2 monolayer domains on Si/SiO_2 sample with corresponding Raman data.

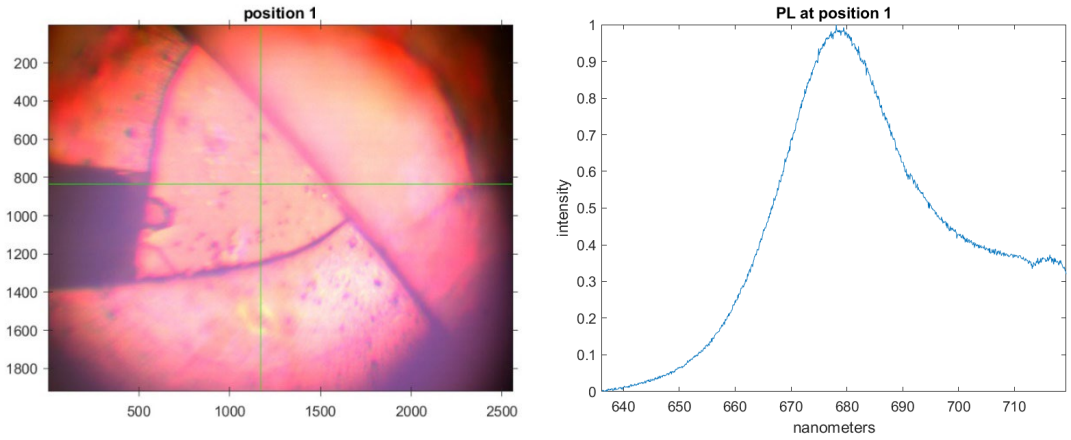

Figure A.3.1: MoS_2 monolayer on DBR with 5nm Al_2O_3 with corresponding PL peak at 680 nm (~1.82 eV).

		F		Cl			Br		I	
step	reaction	E_b	E_r	E_b	E_r	E_{cr}	E_b	E_r	E_b	E_r
1	$MoO_2X_2 + S_2 \rightarrow MoOX_2S_2O$	0.64	−0.25	0.47	−0.39	−0.39	0.44	−0.44	0.38	−0.49
2	$MoOX_2S_2O + S_2 \rightarrow MoOX_2S_2 + S_2O$	0.47	−0.47	0.39	−0.44	−0.83	0.41	−0.45	0.36	−0.46
3	$MoOX_2S_2 + S_2 \rightarrow MoOX_2S + S_3$	0.24	−0.19	0	−0.13	−0.96	0.05	−0.09	0	−0.12
4	$MoOX_2S + S_2 \rightarrow MoX_2SS_2O$	0.67	−0.22	0.53	−0.36	−1.32	0.51	−0.40	0.47	−0.43
5	$MoX_2SS_2O + S_2 \rightarrow MoX_2S_3 + S_2O$	0.52	−0.49	0.44	−0.46	−1.78	0.43	−0.47	0.41	−0.49
6	$MoX_2S_3 + S_2 \rightarrow MoX_2S_2 + S_3$	0.02	−0.23	0	−0.17	−1.95	0	−0.13	0	−0.13
7	$MoX_2S_2 + S_2 \rightarrow MoXS_2S_2X$	0.88	−0.31	0.55	−0.48	−2.43	0.38	−0.61	0.28	−0.83
8	$MoXS_2S_2X + S_2 \rightarrow MoXS_4 + S_2X$	0.58	−0.07	0.17	−0.08	−2.51	0.02	−0.08	0.01	−0.07
9	$MoXS_4 + S_2 \rightarrow MoXS_6$	0	−0.95	0	−0.97	−3.48	0	−1.01	0	−1.06
10	$MoXS_6 + S_2 \rightarrow MoS_6 + S_2X$	0.60	−0.08	0.42	−0.18	−3.66	0.25	−0.25	0.11	−0.37

[a]The reaction barrier and (cumulative) energy are denoted as E_b and $E_{(c)r}$ respectively in eV.

Figure A.3.2: Reaction Table for MoO_3 and MX salts [27].

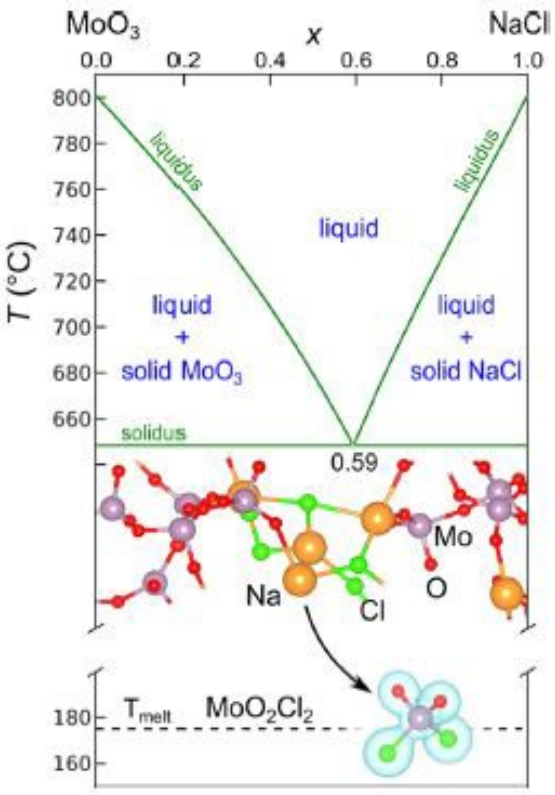

Figure A.3.3: Solid-liquid equilibrium of MoO_3 and NaCl. Eutectic point at 0.59 gives a melting temperature of ~655 ºC. Also, shows melting point of 175 ºC for MoO_2Cl_2 intermediate [27].

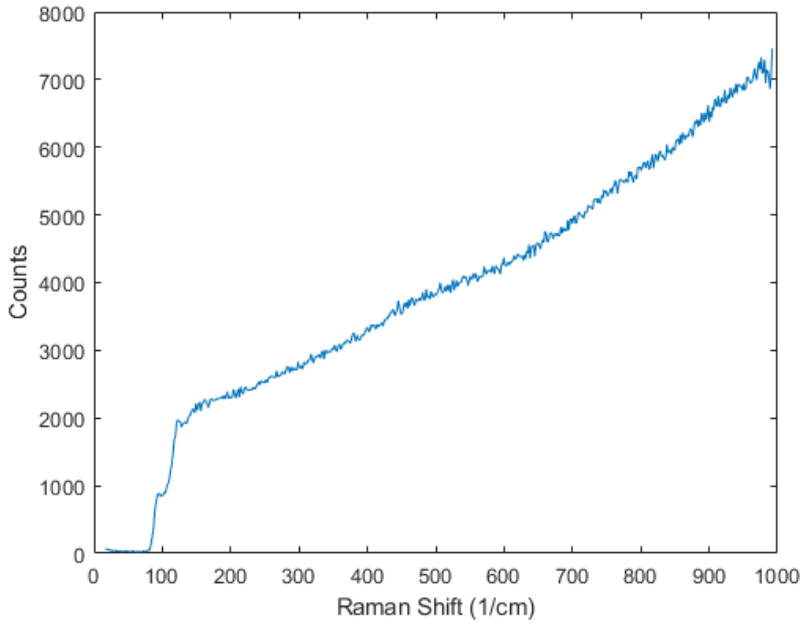

Figure A.3.4: Raman data of blank DBR substrate.

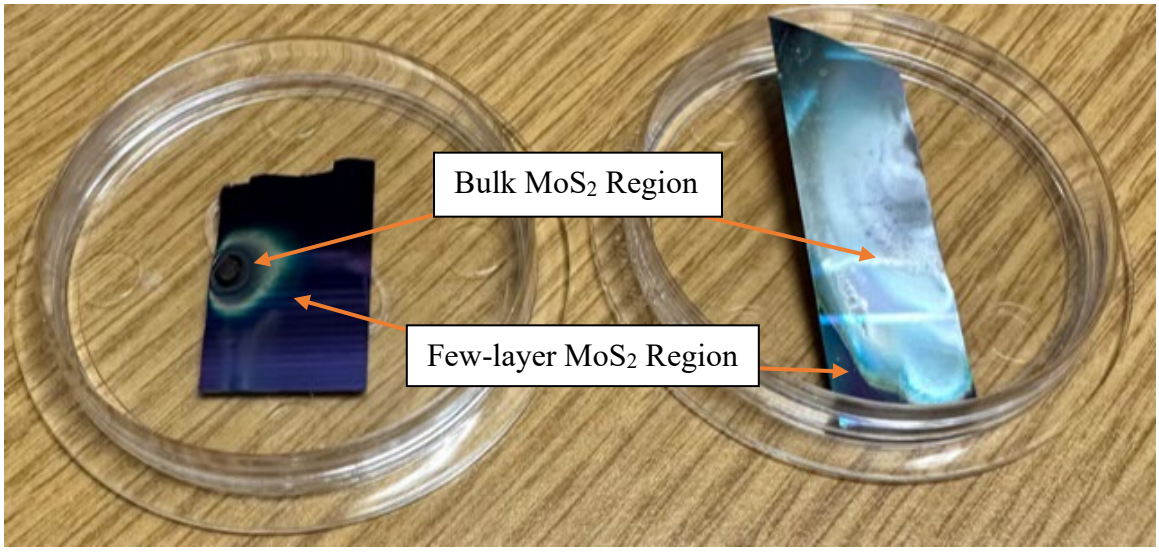

Figure A.4.1: Coffee ring effect of MoS_2. Left is normal growth process; right is salt assisted growth process.

References

[1] H. Deng, H. Haug, and Y. Yamamoto, "Exciton-polariton Bose-Einstein condensation," *Rev. Mod. Phys.*, vol. 82, no. 2, pp. 1489–1537, 2010, doi: 10.1103/RevModPhys.82.1489.

[2] D. W. Snoke and J. Keeling, "The new era of polariton condensates," *Phys. Today*, vol. 70, no. 10, pp. 54–60, 2017, doi: 10.1063/PT.3.3729.

[3] I. Carusotto, "Quantum fluids of light," vol. 85, no. March, 2013, doi: 10.1103/RevModPhys.85.299.

[4] D. N. Basov, M. M. Fogler, and F. J. García De Abajo, "Polaritons in van der Waals materials," *Science (80-.).*, vol. 354, no. 6309, 2016, doi: 10.1126/science.aag1992.

[5] A. S. Davydov, S. B. Dresner, and R. S. Knox, "pulse generator ! Cober," vol. 55, no. 1972, pp. 54–57, 1982, doi: 10.1063/1.3070820.

[6] W. Choi, N. Choudhary, G. H. Han, J. Park, D. Akinwande, and Y. H. Lee, "Recent development of two-dimensional transition metal dichalcogenides and their applications," *Mater. Today*, vol. 20, no. 3, pp. 116–130, 2017, doi: 10.1016/j.mattod.2016.10.002.

[7] A. Splendiani *et al.*, "Emerging photoluminescence in monolayer MoS2," *Nano Lett.*, vol. 10, no. 4, pp. 1271–1275, 2010, doi: 10.1021/nl903868w.

[8] Z. Zeng *et al.*, "Single-layer semiconducting nanosheets: High-yield preparation and device fabrication," *Angew. Chemie - Int. Ed.*, vol. 50, no. 47, pp. 11093–11097, 2011, doi: 10.1002/anie.201106004.

[9] C. Hyun, J. Choi, S. Won, J. Hwa, K. Lee, and J. Ahn, "Synthesis mechanism of MoS 2 layered crystals by chemical vapor deposition using MoO 3 and sulfur powders," *J. Alloys Compd.*, vol. 765, pp. 380–384, 2018, doi: 10.1016/j.jallcom.2018.06.183.

[10] X. Li *et al.*, "Role of hydrogen in the chemical vapor deposition growth of MoS2atomic layers," *Nanoscale*, vol. 7, no. 18, pp. 8398–8404, 2015, doi: 10.1039/c5nr00904a.

[11] L. Wang, Z. L. Xue, A. Huang, and F. F. Wang, "Mechanism and Kinetic Study of Reducing MoO3 to MoO2 with CO-15 vol % CO2 Mixed Gases," *ACS Omega*, vol. 4, no. 22, pp. 20036–20047, 2019, doi: 10.1021/acsomega.9b03171.

[12] X. Zhang, X. F. Qiao, W. Shi, J. Bin Wu, D. S. Jiang, and P. H. Tan, "Phonon and Raman scattering of two-dimensional transition metal dichalcogenides from monolayer, multilayer to bulk material," *Chemical Society Reviews*, vol. 44, no. 9. Royal Society of Chemistry, pp. 2757–2785, 2015, doi: 10.1039/c4cs00282b.

[13] M. Krbal *et al.*, "Amorphous-to-Crystal Transition in Quasi-Two-Dimensional MoS2: Implications for 2D Electronic Devices," *ACS Appl. Nano Mater.*, vol. 4, no. 9, pp. 8834–8844, 2021, doi: 10.1021/acsanm.1c01504.

[14] R. E. Bell and R. E. Herfert, "Preparation and Characterization of a New Crystalline Form of Molybdenum Disulfide," *J. Am. Chem. Soc.*, vol. 79, no. 13, pp. 3351–3354, 1957, doi: 10.1021/ja01570a012.

[15] R. J. Toh, Z. Sofer, J. Luxa, D. Sedmidubský, and M. Pumera, "3R phase of MoS2 and WS2 outperforms the corresponding 2H phase for hydrogen evolution," *Chem. Commun.*, vol. 53, no. 21, pp. 3054–3057, 2017, doi: 10.1039/c6cc09952a.
[16] W. Zhao *et al.*, "Lattice dynamics in mono- and few-layer sheets of WS2 and WSe2," *Nanoscale*, vol. 5, no. 20, pp. 9677–9683, 2013, doi: 10.1039/c3nr03052k.
[17] B. Zheng and Y. Chen, "Controllable Growth of Monolayer MoS2 and MoSe2 Crystals Using Threeerature-zone Furnace," *IOP Conf. Ser. Mater. Sci. Eng.*, vol. 274, no. 1, pp. 0–6, 2017, doi: 10.1088/1757-899X/274/1/012085.
[18] Y. Yu, C. Li, Y. Liu, L. Su, Y. Zhang, and L. Cao, "Controlled scalable synthesis of uniform, high-quality monolayer and few-layer MoS2 films," *Sci. Rep.*, vol. 3, pp. 1–6, 2013, doi: 10.1038/srep01866.
[19] M. Velický *et al.*, "Photoelectrochemistry of Pristine Mono- and Few-Layer MoS2," *Nano Lett.*, vol. 16, no. 3, pp. 2023–2032, 2016, doi: 10.1021/acs.nanolett.5b05317.
[20] Y. Okuno *et al.*, "Probing the nanoscale light emission properties of a CVD-grown MoS2 monolayer by tip-enhanced photoluminescence," *Nanoscale*, vol. 10, no. 29, pp. 14055–14059, 2018, doi: 10.1039/c8nr02421a.
[21] G. Plechinger *et al.*, "A direct comparison of CVD-grown and exfoliated MoS 2 using optical spectroscopy," no. 100, pp. 1–7.
[22] Virgina Semiconductor, "The General Properties of Si, Ge, SiGe, SiO2 and Si3N4," 2002.
[23] T. Scientific, "FTIR Basics." https://www.thermofisher.com/us/en/home/industrial/spectroscopy-elemental-isotope-analysis/spectroscopy-elemental-isotope-analysis-learning-center/molecular-spectroscopy-information/ftir-information/ftir-basics.html.
[24] S. Jiménez Sandoval, D. Yang, R. F. Frindt, and J. C. Irwin, "Raman study and lattice dynamics of single molecular layers of MoS2," *Phys. Rev. B*, vol. 44, no. 8, pp. 3955–3962, 1991, doi: 10.1103/PhysRevB.44.3955.
[25] G. S. Higashi and C. G. Fleming, "Sequential surface chemical reaction limited growth of high quality Al 2O3 dielectrics," *Appl. Phys. Lett.*, vol. 55, no. 19, pp. 1963–1965, 1989, doi: 10.1063/1.102337.
[26] H. Zhang, "Nucleation and Growth Mechanisms of 2D Semiconductor/high-k Dielectric Heterostacks," Ku Leuven, 2018.
[27] J. Lei, Y. Xie, A. Kutana, K. V. Bets, and B. I. Yakobson, "Salt-Assisted MoS2Growth: Molecular Mechanisms from the First Principles," *J. Am. Chem. Soc.*, vol. 144, no. 16, pp. 7497–7503, 2022, doi: 10.1021/jacs.2c02497.
[28] A. M. Van Der Zande *et al.*, "Grains and grain boundaries in highly crystalline monolayer molybdenum disulphide," *Nat. Mater.*, vol. 12, no. 6, pp. 554–561, 2013, doi: 10.1038/nmat3633.